1-1-2018

Porous NaTi2(PO4)(3) Nanocubes Anchored on Porous Carbon Nanosheets for High Performance Sodium-Ion Batteries

Ziqi Wang
Hunan University

Jiaojiao Liang
Hunan University

Kai Fan
Hunan University

Xiaodi Liu
Hunan University , Nanyang Normal University

Caiyun Wang
University of Wollongong, caiyun@uow.edu.au

See next page for additional authors

Porous NaTi2(PO4)(3) Nanocubes Anchored on Porous Carbon Nanosheets for High Performance Sodium-Ion Batteries

Abstract

NaTi2(PO4)3 has attracted great interest as anode material for sodium ion batteries owing to its open three-dimensional framework structure and limited volume changes during the charge and discharge process. However, the poor intrinsic electronic conductivity of NaTi2(PO4)3 needs to be improved for high rate capability. In this work, porous NaTi2(PO4)3 nanocubes anchored on porous carbon nanosheets (NaTi2(PO4)3/C) are designed and developed. This material exhibits a large discharge capacity and good rate capacity including a first discharge capacity of 485 mAh g−1 at a current density of 0.1 A g−1, and 98 mAh g−1 retained at a high rate of 4 A g−1 even after 2,000 cycles. These results suggest that NaTi2(PO4)3/C is a promising anode material for sodium-ion batteries.

Keywords

batteries, porous, sodium-ion, high, performance, nati2(po4)(3), nanocubes, anchored, carbon, nanosheets

Disciplines

Engineering | Physical Sciences and Mathematics

Publication Details

Wang, Z., Liang, J., Fan, K., Liu, X., Wang, C. & Ma, J. (2018). Porous NaTi2(PO4)(3) Nanocubes Anchored on Porous Carbon Nanosheets for High Performance Sodium-Ion Batteries. Frontiers in Chemistry, 6 396-1-396-8.

Authors

Ziqi Wang, Jiaojiao Liang, Kai Fan, Xiaodi Liu, Caiyun Wang, and Jianmin Ma

frontiers in Chemistry

ORIGINAL RESEARCH
published: 19 September 2018
doi: 10.3389/fchem.2018.00396

Porous $NaTi_2(PO_4)_3$ Nanocubes Anchored on Porous Carbon Nanosheets for High Performance Sodium-Ion Batteries

Ziqi Wang[1], Jiaojiao Liang[1], Kai Fan[1], Xiaodi Liu[1,2], Caiyun Wang[3]* and Jianmin Ma[1,4]**

[1] School of Physics and Electronics, Hunan University, Changsha, China, [2] College of Chemistry and Pharmaceutical Engineering, Nanyang Normal University, Nanyang, China, [3] ARC Centre of Excellence for Electromaterials Science, Intelligent Polymer Research Institute, AIIM Facility, University of Wollongong, North Wollongong, NSW, Australia, [4] Institute of Advanced Electrochemical Energy, Xi'an University of Technology, Xi'an, China

OPEN ACCESS

Edited by:
Qiaobao Zhang,
Xiamen University, China

Reviewed by:
Chao Lai,
Jiangsu Normal University, China
Guiming Zhong,
Fujian Institute of Research on the Structure of Matter (CAS), China
Anmin Cao,
Institute of Chemistry (CAS), China

***Correspondence:**
Xiaodi Liu
liuxiaodiny@126.com
Caiyun Wang
caiyun@uow.edu.au
Jianmin Ma
nanoelechem@hnu.edu.cn

Specialty section:
This article was submitted to Nanoscience, a section of the journal Frontiers in Chemistry

Received: 05 June 2018
Accepted: 16 August 2018
Published: 19 September 2018

Citation:
Wang Z, Liang J, Fan K, Liu X, Wang C and Ma J (2018) Porous $NaTi_2(PO_4)_3$ Nanocubes Anchored on Porous Carbon Nanosheets for High Performance Sodium-Ion Batteries. Front. Chem. 6:396. doi: 10.3389/fchem.2018.00396

$NaTi_2(PO_4)_3$ has attracted great interest as anode material for sodium ion batteries owing to its open three-dimensional framework structure and limited volume changes during the charge and discharge process. However, the poor intrinsic electronic conductivity of $NaTi_2(PO_4)_3$ needs to be improved for high rate capability. In this work, porous $NaTi_2(PO_4)_3$ nanocubes anchored on porous carbon nanosheets ($NaTi_2(PO_4)_3$/C) are designed and developed. This material exhibits a large discharge capacity and good rate capacity including a first discharge capacity of 485 mAh g^{-1} at a current density of 0.1 A g^{-1}, and 98 mAh g^{-1} retained at a high rate of 4 A g^{-1} even after 2,000 cycles. These results suggest that $NaTi_2(PO_4)_3$/C is a promising anode material for sodium-ion batteries.

Keywords: $NaTi_2(PO_4)_3$, nanocubes, carbon nanosheets, anode, sodium-ion batteries

INTRODUCTION

Sodium-ion batteries (SIBs), as an alternative energy storage system for lithium-ion batteries (LIBs), have attracted increasing attention due to their low cost and the abundant resource of sodium (Gao et al., 2017; Cui et al., 2018; Liang et al., 2018c). The electrochemical performance of SIBs is closely related to the properties of electrode materials, especially anode materials (Chen et al., 2018; Fan et al., 2018; Hu A. J. et al., 2018; Liang et al., 2018b,d; Wan et al., 2018; Wei et al., 2018). Recently, Na super ion conductor (NASICON) type $NaTi_2(PO_4)_3$ has been considered as one of promising anode materials for SIBs owing to its "zero-stress" three-dimensional (3D) framework, high Na^+ conductivity, and good thermal stability (Kabbour et al., 2011; Wu et al., 2013; Sun et al., 2016; Ye et al., 2017).

However, the poor intrinsic electrical conductivity of NTP leads to poor rate capability (Pang et al., 2014b; Roh et al., 2017). To improve the Na^+ ions insertion-extraction kinetics, two common approaches used include synthesis of various nanostructures and fabrication of carbon composites. Morphology control of $NaTi_2(PO_4)_3$ has been applied to realizeexcellent electrochemical performance. Different nanostructures such as hollow nanocubes, nanoparticles, and hierarchical microspheres have been demonstrated (Wu et al., 2015; Fang et al., 2016; Ye et al., 2017). Among them, porous structures have gained great attention owing to the afforded large surface areas and improved kinetics (Dirican et al., 2015; Zhang et al., 2017; Zhao et al., 2017; Zhou et al., 2017). Moreover, the electronic conductivity of anodes can be largely enhanced by hybridizing

them with conductive materials. For example, the coating of carbon or graphene on $NaTi_2(PO_4)_3$ micro/nanostructures can effectively improve their properties and higher quality of the conductive materials could result in better electrochemical performance. Nevertheless, the contents of carbon or graphene in the previously reported composites were only 3.4–6.8 wt% (Pang et al., 2014b; Fang et al., 2016; Geng et al., 2017; Hu Q. et al., 2018; Liang et al., 2018a). Thus, to obtain better electrochemical properties, the contents of conduction materials should be increased. It has been found that the embedding of anode materials in carbon/graphene matrixes can realize high content of conductive carbon materials for enhanced electrochemical properties (Fu et al., 2015; Guo et al., 2015; Choi et al., 2016; Sun et al., 2016). Motivated by the above potentials, we have prepared porous $NaTi_2(PO_4)_3$ nanocubes anchored on porous carbon nanosheets ($NaTi_2(PO_4)_3$/C) through ultrasonic treatment. To the best of our knowledge, it is the first report that $NaTi_2(PO_4)_3$ nanocubes with porous structures have been embedded in a porous carbon matrix. This $NaTi_2(PO_4)_3$/C material exhibited a high discharge capacity, good rate performance, and excellent long-time cycling stability.

EXPERIMENTAL SECTION

Synthesis of $NaTi_2(PO_4)_3$/C

The synthesis of porous carbon nanosheets was firstly conducted from the uniform mixture of $Zn(CH_3COO)_2{\cdot}2H_2O$ (5 g) and oleic acid (5 g) in an agate mortar for 30 min. Then the above mixture was transferred into a tubular furnace and calcined at 700°C for 2 h with a ramping rate of 2°C min^{-1} in Ar atmosphere to form ZnO/C slices. The ZnO/C slices were washed using 6 mol L^{-1} aqueous HCl solution to form porous carbon nanosheets. These carbon nanosheets were washed by deionized water and absolute ethanol, then dried in vacuum at 50°C for 8 h. Similar process was used to prepare the MnO/graphene composite using oleic acid as carbon sources (Guo et al., 2015).

The synthesis of $NaTi_2(PO_4)_3$ nanocubes was conducted following the reported procedures (Wu et al., 2015). Briefly, sodium acetate (0.16 g) was added in a mixed solvent glacial acetic acid (0.7 mL), phosphoric acid (4 ml) and ethylene glycol (25 ml), followed by the addition of tetrabutyl titanate (1.36 g). The resultant mixture was heated at 180°C for 12 h. Finally, the white precipitate $NaTi_2(PO_4)_3$ was obtained.

For synthesizing $NaTi_2(PO_4)_3$/C, 0.16 g precursor $NaTi_2(PO_4)_3$, 0.04 g porous carbon nanosheets, and 3.6 g cetyltrimethylammonium bromide (CTAB) were added into 30 mL absolute ethanol. After being stirred for 2 h and ultrasonically dispersed for 2 h, the precursor $NaTi_2(PO_4)_3$/C was collected by centrifugation, washed with deionized water and anhydrous ethanol, and dried at 60°C for 12 h. Subsequently, the precursor $NaTi_2(PO_4)_3$/C was further calcined at 700°C for 2 h with a ramping rate of 2°C min^{-1} in Ar atmosphere to form $NaTi_2(PO_4)_3$/C. For comparison, porous $NaTi_2(PO_4)_3$ cubes were prepared after annealing without the porous carbon nanosheets.

Characterizations

Rigaku D/max-2500 X-ray diffractometer (Cu Kα, $\lambda = 1.54056$ Å) was used to investigate the crystal structures. The morphology and nanostructure were observed by Hitachi S4800 scanning electron microscopy and JEOL 2010 transmission electron microscopy. The Brunauer-Emmett-Teller special (BET) surface area and pore size were tested at 77 K on a Nova 2000e volumetric adsorption analyzer. The thermogravimetric (TG) analysis was performed with a WCT-1D instrument over a range of 30–800°C at a heating rate of 10°C·min^{-1} in air atmosphere.

Electrochemical Measurements

Active materials, acetylene black and carboxymethylcellulose sodium with a weight ratio of 80:10:10 were uniformly mixed, and the obtained slurry was coated on Cu foil. Then, the electrodes were assembled into CR2025 coin cell in the glove box. The glass microfiber filter membrane (Whatman, grade GF/A) was used as the separator. Metallic sodium film was used as counter/reference electrodes. The electrolyte was 1 mol L^{-1} $NaClO_4$ dissolved in a mixture of ethylene carbonate and diethyl carbonate (1:1 vol%) with 5 wt% fluoroethylene carbonate. Galvanostatic tests were evaluated by Neware Battery Testing System. Cyclic voltammetry (CV) tests and impedance measurement were carried out on a CHI660C Electrochemical Workstation.

RESULTS AND DISCUSSION

The phase of $NaTi_2(PO_4)_3$ and $NaTi_2(PO_4)_3$/C were confirmed by XRD, as shown in **Figure 1A**. All diffraction peaks are in accordance with the standard pattern of $NaTi_2(PO_4)_3$ (JCPDS No. 84-2008). No peaks for impurities can be detected, suggesting the high purity of these two samples. Moreover, the diffraction peaks of carbon material is not clearly discerned due to the sharp and strong diffraction of $NaTi_2(PO_4)_3$, implying the high crystalline nature. In addition, according to the TGA curve of $NaTi_2(PO_4)_3$ (**Figure 1B**), the relative weight fraction of carbon for $NaTi_2(PO_4)_3$/C was determined to be ∼18.3%.

The morphology of porous carbon nanosheets, $NaTi_2(PO_4)_3$, and $NaTi_2(PO_4)_3$/C was characterized by SEM. **Figure 2A** shows the low-magnified SEM image of porous carbon nanosheets. It is clear that the sample is exclusively nanosheets with irregular morphologies. The high-resolution SEM image (**Figure 2B**) shows that the carbon nanosheets are curved and have an average thickness of ∼10 nm. SEM images of $NaTi_2(PO_4)_3$ (**Figures 2C,D**) show that the products have uniform cubic shapes and their sizes are in the range between 50 and 100 nm, similar with the results reported in literatures (Liang et al., 2018a).

It was observed that the $NaTi_2(PO_4)_3$ were uniformly anchored on the porous carbon nanosheets for $NaTi_2(PO_4)_3$/C sample (**Figures 3A,B**). The detailed structural characteristics of $NaTi_2(PO_4)_3$/C was further investigated by TEM. The TEM image in **Figure 3C** illustrates that $NaTi_2(PO_4)_3$ in a size range of 50 and 100 nm were scattered over the carbon nanosheets. This is consistent with the SEM results in **Figure 3B**. Notably, both nanocubes and carbon nanosheets have obvious porous structure, which is beneficial for the transport of

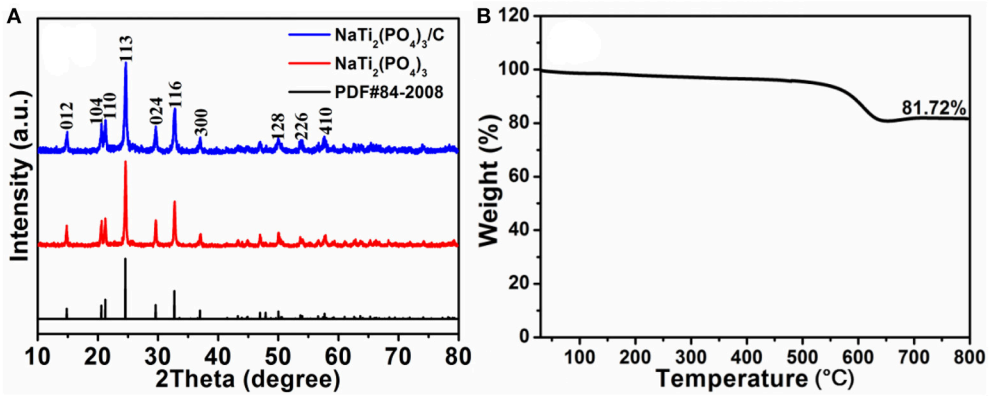

FIGURE 1 | (A) XRD patterns of $NaTi_2(PO_4)_3$ and $NaTi_2(PO_4)_3$/C; **(B)** TG curve of $NaTi_2(PO_4)_3$/C.

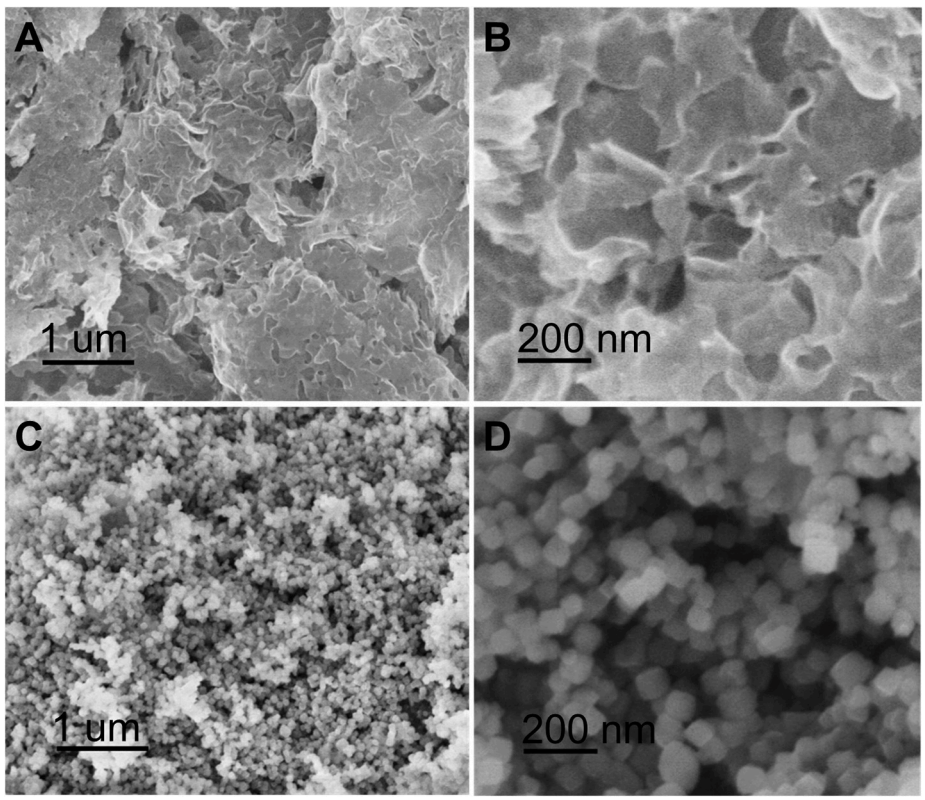

FIGURE 2 | (A) SEM image and **(B)** high-resolution SEM image of porous carbon nanosheets; **(C)** SEM image and **(D)** high-magnification SEM image of $NaTi_2(PO_4)_3$.

Na^+ (Wu et al., 2015). Additionally, the HR-TEM image of a representative nanocube (**Figure 3D**) implies that the interplanar spacing is *ca.* 0.365 nm, in good agreement with the (113) plane of NASICON-type phase (Ye et al., 2017).

BET analysis was performed to study the pore size and specific surface area of $NaTi_2(PO_4)_3$/C. The Nitrogen adsorption-desorption isotherm of $NaTi_2(PO_4)_3$/C (**Figure 4A**) reveals a type-IV isotherm with an obvious H1-type hysteretic loop in the range of 0.4–1.0 (P/P_0), indicating that the products possess porous structures (Takashima et al., 2015). The BET analysis indicates that the specific surface area of $NaTi_2(PO_4)_3$/C was *ca.* 103.1 $m^2\ g^{-1}$. Moreover, as shown in **Figure 4B**, the sample possessed a broad pore-size distribution and the pore-size distribution maximum was centered at 15.4 nm. The large surface area and porous structure of $NaTi_2(PO_4)_3$/C is beneficial to improve the sodium-ion storage properties (Wang H. et al., 2016; Wang G. et al., 2018).

The electrochemical properties of $NaTi_2(PO_4)_3$/C were studied as anode material for SIBs. The cyclic voltammogram (CV) of $NaTi_2(PO_4)_3$/C at a scan rate of 0.1 mV s^{-1} was analyzed

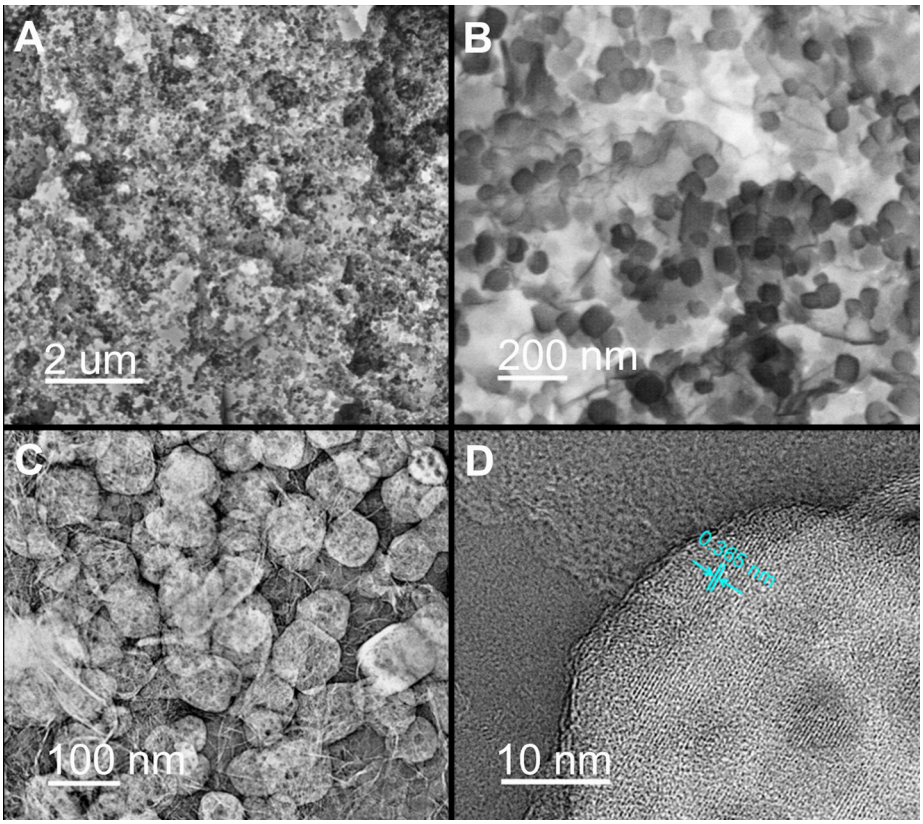

FIGURE 3 | (A) SEM image, **(B)** high-resolution SEM image, and **(C)** TEM image of $NaTi_2(PO_4)_3$/C; **(D)** HR-TEM images of a typical $NaTi_2(PO_4)_3$ particle anchored on carbon nanosheets.

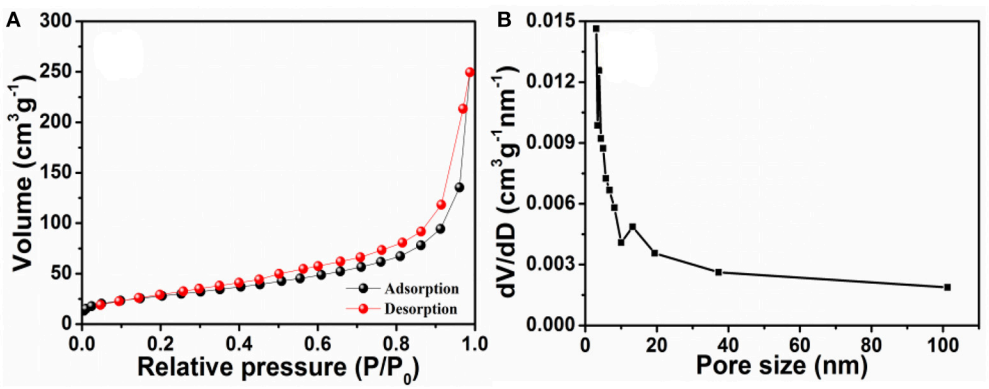

FIGURE 4 | (A) N_2 adsorption-desorption isotherm and **(B)** pore-size distribution curve of $NaTi_2(PO_4)_3$/C.

to investigate their redox kinetic properties. In **Figure 5A**, at the 1st cycle, a pair of redox peaks at 1.97/2.29 V can be attributed to conversion reaction of Ti^{4+}/Ti^{3+} (Pang et al., 2014a; Fang et al., 2016; Ye et al., 2017). Moreover, another pair of cathodic/anodic peaks located at 0.27/0.57 V can be attributed to the redox reaction between Ti^{3+} and Ti^{2+} (Senguttuvan et al., 2013; Wang D. et al., 2016). That is, Ti^{4+} in the reduction process was firstly reduced to Ti^{3+} ($NaTi_2(PO_4)_3 + 2Na^+ + 2e^- \rightarrow Na_3Ti_2(PO_4)_3$) and then formed into Ti^{2+} ($Na_3Ti_2(PO_4)_3 + Na^+ + e^- \rightarrow Na_4Ti_2(PO_4)_3$). In the following cycles, the anodic peaks shift to higher potentials (1.97 vs. 2.09 V; 0.27 vs. 0.30 V), which was probably caused by the stress/strain change, similar to other NASICON-type anodic materials (Li et al., 2014). More importantly, in the following 2nd, 3rd, and 5th cycles, two pairs of reduction/oxidation peaks almost remained unchanged, indicating the excellent reversibility.

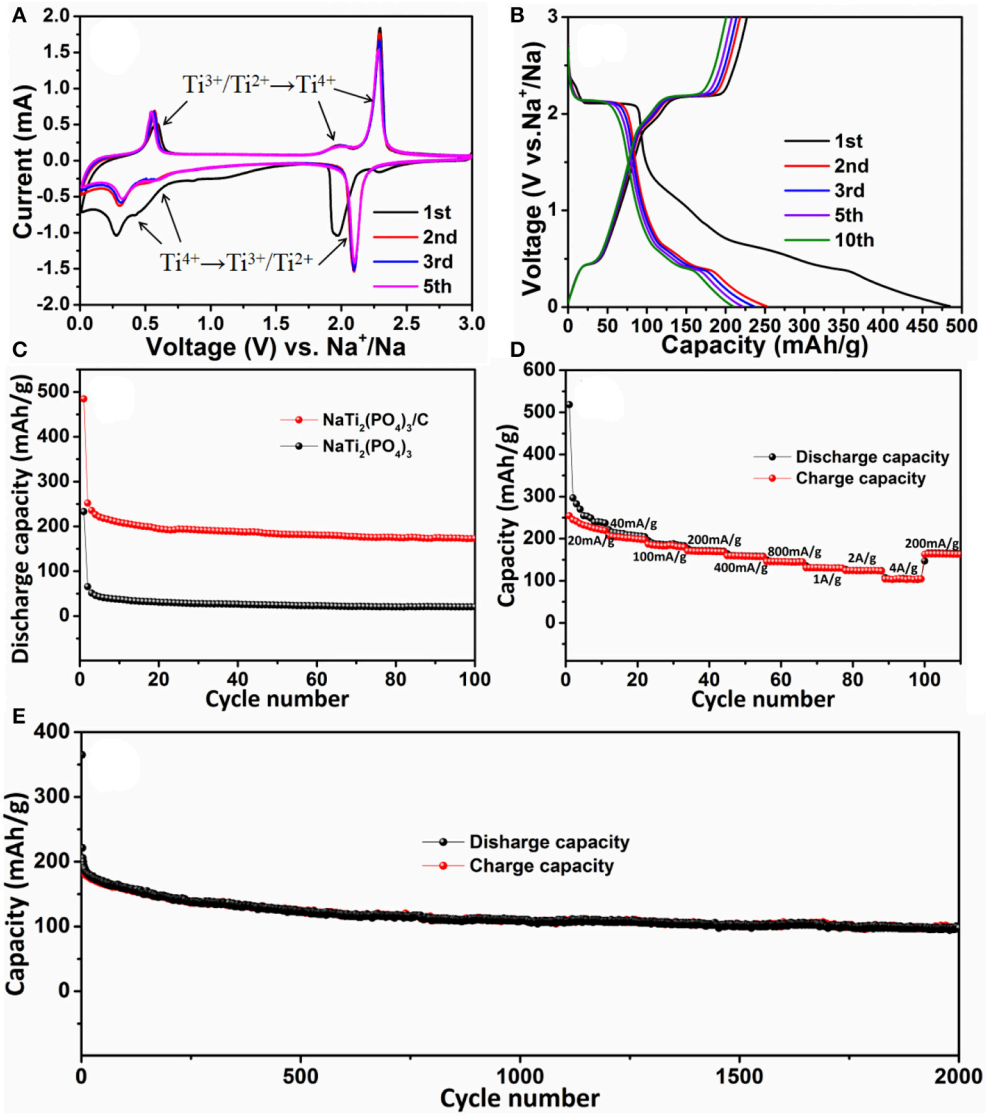

FIGURE 5 | (A) Cyclic voltammogram curves of $NaTi_2(PO_4)_3$/C for the initial five cycles in the voltage range of 0.01–3.0 V (vs. Na^+/Na); **(B)** discharge-charge curves of $NaTi_2(PO_4)_3$/C at a current density of 0.1 A g^{-1}; **(C)** cycling performances of $NaTi_2(PO_4)_3$/C and $NaTi_2(PO_4)_3$ at 0.1 A g^{-1}; **(D)** rate capacity of $NaTi_2(PO_4)_3$/C; **(E)** long-term cycling performance of $NaTi_2(PO_4)_3$/C at a high rate of 4 A g^{-1}.

Figure 5B showed the galvanostatic discharge-charge curves of $NaTi_2(PO_4)_3$/C electrode in the voltage window between 0.01 and 3.0 V. The initial discharge capacity was 485 mAh g^{-1}, which was higher than the theoretical capacity (133 mAh g^{-1}). However, the initial charge capacity was 227 mAh g^{-1} with an unsatisfied Coulombic efficiency of 46.8%. Such a large capacity loss is mostly ascribed to the formation of solid electrolyte interface (SEI) layers for the existence of carbon substrates, as well as the decomposition of electrolyte (Hasegawa et al., 2016; Wang D. et al., 2016). On the contrary, the first discharge capacity of the $NaTi_2(PO_4)_3$ electrode was only 229 mAh g^{-1} (**Figure S1**, Supporting Information). In the subsequent cycles, the $NaTi_2(PO_4)_3$/C electrode possessed good cycle stability and excellent reversibility for Na^+ ion insertion and extraction. For example, at the 5th and 10th cycles, the discharge capacity retained to be 221 and 203 mAh g^{-1} with the coulombic efficiency of 94 and 96%, respectively. **Figure 5C** displayed the cycling behavior of the $NaTi_2(PO_4)_3$/C and $NaTi_2(PO_4)_3$ electrodes at a current density of 0.1 A g^{-1}. It can be seen thatafter 100 cycle $NaTi_2(PO_4)_3$/C still delivered a discharge capacity of 172 mAh g^{-1}, which was much larger than that of $NaTi_2(PO_4)_3$ (20 mAh g^{-1}). Accordingly, the $NaTi_2(PO_4)_3$/C electrode exhibited a capacity retention of 69% (relative to the 2nd cycle), higher than that of $NaTi_2(PO_4)_3$ (30%). In addition, the long-term cycling performance for the $NaTi_2(PO_4)_3$/C electrode at a relatively high rate of 4 A g^{-1} was further studied. In **Figure 5E**, it can be clearly found that the Coulombic efficiency could

exceed 98% since the 10th cycle, and the electrode can still maintain a discharge capacity of 98 mAh g^{-1} even after 2,000 cycles. All these results indicate that $NaTi_2(PO_4)_3$/C afforded improved electrochemical stability compared with that of $NaTi_2(PO_4)_3$.

Furthermore, the rate capability of $NaTi_2(PO_4)_3$/C electrode was also investigated by increasing rate from 0.02 to 4 A g^{-1} and back to 0.2 A g^{-1}. As illustrated in **Figure 5D**, the discharge capability of $NaTi_2(PO_4)_3$/C was 280 mAh g^{-1} at 0.02 A g^{-1}, and then it slowly decreased with the increasing current density. When the current density was reversed to 0.2 A g^{-1}, a capacity of 164 mAh g^{-1} could be restored. Obviously, $NaTi_2(PO_4)_3$/C has excellent rate capacity.

Lastly, EIS measurements were carried out to further study the surface reaction activities of $NaTi_2(PO_4)_3$/C and $NaTi_2(PO_4)_3$. Before the EIS tests, the coin cells were cycled three times in the voltage range of 1.0–2.5 V, and the corresponding Nyquist plots are shown in **Figure 6**. It can be seen that each Nyquist plot exhibited a semicircle at high frequency region and a straight line at low frequency region. The surface charge-transfer resistance (R_{ct}) of $NaTi_2(PO_4)_3$/C was found to be smaller than that of $NaTi_2(PO_4)_3$, suggesting that the diffusion of Na^+ in $NaTi_2(PO_4)_3$/C is faster than $NaTi_2(PO_4)_3$ (Lu et al., 2014; Longoni et al., 2016). In addition, the Na^+ diffusion coefficient (D) can be calculated by the following equations (Ko et al., 2017):

$$D = R^2T^2/2A^2n^4F^4C^4\sigma^2 \quad (1)$$

$$Z' = R_o + R_{ct} + \sigma\omega^{-0.5} \quad (2)$$

in which R is the ideal gas constant, T is the ambient temperature, A is the surface area of the electrode, n is the number of electrons per molecule during intercalation, F is the Faraday constant, C is the concentration of Na^+ in the active material, σ is the Warburg coefficient, Z' is the real part of the impedance, ω is the angular frequency. The σ value can be calculated by the slope of the plot of Z' vs. $\omega^{-0.5}$ and presented in **Figure S2**. The σ value of $NaTi_2(PO_4)_3$/C was 254 Ω $s^{-0.5}$, much lower than that of $NaTi_2(PO_4)_3$ (1264 Ω $s^{-0.5}$). Accordingly D of $NaTi_2(PO_4)_3$/C was larger than that of $NaTi_2(PO_4)_3$. Summarily, $NaTi_2(PO_4)_3$/C can effectively restrain the increasing of charge-transfer resistance after multiple discharge and charge cycles, which can improve the rate capability and enhance the cyclic performance at high rate (Song et al., 2014; Roy and Srivastava, 2015).

According to the above results, $NaTi_2(PO_4)_3$/C has high discharge capacity, good rate capacity, and excellent long-term cycling stability. In addition, compared to other previously reported $NaTi_2(PO_4)_3$@C composites, the obtained $NaTi_2(PO_4)_3$/C electrode exhibits excellent properties (**Table S1**, Supporting Information). The good properties of $NaTi_2(PO_4)_3$/C could be ascribed to the following reasons: (i) The crystal structure of NASICON-type $NaTi_2(PO_4)_3$ is an open 3D framework of PO_4 tetrahedra corner-shared with TiO_6 octahedra, which can not only provide large spaces for Na^+ insertion but also supply open tunnels for Na^+ transport (Boilot et al., 1983; Pang et al., 2014b; Zhao et al., 2015). (ii)

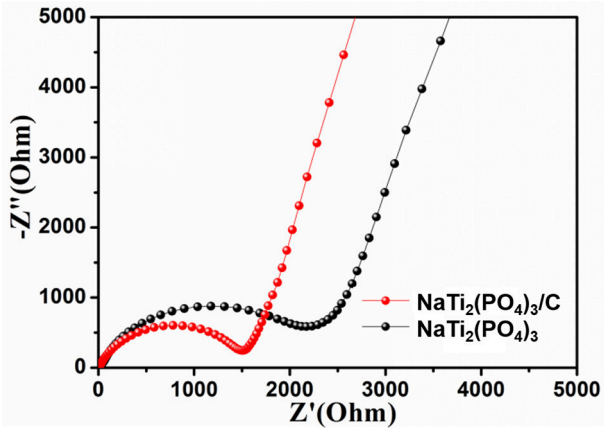

FIGURE 6 | Nyquist plots of $NaTi_2(PO_4)_3$/C and $NaTi_2(PO_4)_3$.

The porous structure of nanostructured $NaTi_2(PO_4)_3$ and carbon matrix can decrease the diffusion length of Na^+ (Gibaud et al., 1996; Huang et al., 2015; Rui et al., 2016). (iii) The embedding of $NaTi_2(PO_4)_3$ nanocubes in carbon nanosheets can effectively inhibit the aggregation of the nanocubes, leading to the electrolyte easily penetrating to the active sites.

CONCLUSION

In summary, the composition of $NaTi_2(PO_4)_3$ porous nanocubes and carbon porous nanosheet are successfully developed. The as-obtained $NaTi_2(PO_4)_3$/C electrodes have good electrochemical properties, including large energy density, excellent rate capacity, and good cycling performance, owing to their special structures and components. The results demonstrate that such $NaTi_2(PO_4)_3$/C anode is a promising anode for SIBs.

AUTHOR CONTRIBUTIONS

ZW, XL, CW, and JM design the whole experiment, and write the paper. JL and KF conduct some electrochemical analysis.

FUNDING

This work is supported by the National Natural Science Foundation of China (No. 21501101), the China Postdoctoral Science Foundation (No. 2017M622564), the Program for Science and Technology Innovation Talents in Universities of Henan Province (No. 15HASTIT007), and the Natural Science Foundation of Hunan Province (2017JJ1008).

SUPPLEMENTARY MATERIAL

The Supplementary Material for this article can be found online at: https://www.frontiersin.org/articles/10.3389/fchem.2018.00396/full#supplementary-material

REFERENCES

Boilot, J. P., Collin, G., and Comes, R. (1983). Zirconium deficiency in nasicon-type compounds: crystal structure of $Na_5Zr(PO_4)_3$. *J. Solid State Chem.* 50, 91–99. doi: 10.1016/0022-4596(83)90236-0

Chen, K. N., Wang, Q. R., Niu, Z. Q., and Chen, J. (2018). Graphene-based materials for flexible energy storage devices. *J. Energy Chem.* 27, 12–24. doi: 10.1016/j.jechem.2017.08.015

Choi, J. H., Ha, C. W., Choi, H. Y., Shin, H. C., Park, C. M., Lee, S. M. (2016). Sb_2S_3 embedded in amorphous P/C composite matrix as high-performance anode material for sodium ion batteries. *Electrochim. Acta* 210, 588–595. doi: 10.1016/j.electacta.2016.05.190

Cui, C. Y., Wei, Z. X., Xu, J. T., Zhang, Y. Q., Liu, S. H., and Dou, S. X. (2018). Three-dimensional carbon frameworks enabling MoS_2 as anode for dual ion batteries with superior sodium storage properties. *Energ. Storage Mater.* 15, 22–30. doi: 10.1016/j.ensm.2018.03.011

Dirican,M., Lu,Y., Ge, Y., Yildiz, O., and Zhang, X. (2015). Carbon-confined SnO_2-electrodeposited porous carbon nanofiber composite as high-capacity sodium-ion battery anode material. *ACS Appl. Mater. Inter* 7, 18387–18396. . doi: 10.1021/acsami.5b04338

Fan, H. S., Yu, H., Zhang, Y. F., Guo, J., Wang, Z., and Xu, J. (2018). 1D to 3D hierarchical iron selenide hollow nanocubes assembled from $FeSe_2$@C core-shell nanorods for advanced sodium ion batteries. *Energ. Storage Mater.* 10, 48–55. doi: 10.1016/j.ensm.2017.08.006

Fang, Y., Xiao, L., Qian, J., Cao, Y., Ai, X., Huang, Y., et al. (2016). Three-dimensional graphene decorated NaTi2(PO4)3 microspheres as a superior high-rate and ultra cycle-stable anode material for sodium ion batteries. *Adv. Energ. Mater.* 6:1502197. doi: 10.1002/aenm.201502197

Fu, Y., Zhang, Z., Yang, X., Gan, Y., and Chen W. (2015). ZnS nanoparticles embedded in porous carbon matrices as anode materials for lithium ion batteries. *RSC Adv.* 5, 86941–86944. doi: 10.1039/C5RA15108B

Gao, Y., Chen, K., Chen, H. M., Hu, X. H., Deng, Z. H., and Wei, Z. D. (2017). Surfactant assisted solvothermal synthesis of $LiFePO_4$ nanorods for lithium-ion batteries. *J. Energy Chem.* 26, 564–568. doi: 10.1016/j.jechem.2016.10.016

Geng, H., Yang, J., Yu, H., Li, C., and Dong, X. (2017). Carbon intercalated porous $NaTi_2(PO_4)_3$ spheres as high-rate and ultralong-life anodes for rechargeable sodium-ion batteries. *Mater. Chem. Front.* 1, 1435–1440. doi: 10.1039/C7QM00048K

Gibaud, A., Xue, J.S., and Dahn, J. R. (1996). Influence of the carbonization heating rate on the physical properties of activated carbons from a sub-bituminous coal. *Carbon* 34, 499–503. doi: 10.1016/0008-6223(95)00207-3

Guo, W., Li, X., Ng, D. H. L., and Ma, J. M. (2015). Integration of MnO@graphene with graphene networks towards Li-ion battery anodes. *RSC Adv.* 5, 96681–96684. doi: 10.1039/C5RA18927F

Hasegawa, G., Kanamori, K., Kannari, N., Ozaki, J. I., Nakanishi, K., Abe, T. (2016). Studies on electrochemical sodium storage into hard carbons with binder-free monolithic electrodes. *Power Sourc. J.* 318, 41–48. doi: 10.1016/j.jpowsour.2016.04.013

Hu, A. J., Jin, S., Du, Z. Z., Jin, H. C., and Ji, H. X. (2018). NS codoped carbon nanorods as anode materials for high-performance lithium and sodium ion batteries. *J. Energ. Chem.* 27, 203–208. doi: 10.1016/j.jechem.2017.11.022

Hu, Q., Yu, M., Liao, J., Wen, Z., and Chen, C. (2018). Porous carbon-coated $NaTi_2(PO_4)_3$ with superior rate and low-temperature properties. *J. Mater. Chem. A* 6, 2365–2370. doi: 10.1039/C7TA10207K

Huang, L., Cheng, J., Li, X., and Wang, B. (2015). Electrode nanomaterials for room temperature sodium-ion batteries: a review. *J. Nanosci. Nanotechno.* 15, 6295–6307. doi: 10.1166/jnn.2015.11122

Kabbour, H., Coillot, D., Colmont, M., Masquelier, C., and Mentré, O. (2011). α-$Na_3M_2(PO_4)_3$ (M = Ti, Fe): Absolute cationic ordering in NASICON-type phases. *J. Am. Chem. Soc.* 133, 11900–11903. doi: 10.1021/ja204321y

Ko, J. S., Doan-Nguyen, V. V., T., Kim, H. S., Petrissans, X., DeBlock, R. H., Dunn, B. S. (2017). High-rate capability of Na_2FePO_4F nanoparticles by enhancing surface carbon functionality for Na-ion batteries. *J. Mater. Chem. A* 5, 18707–18715. doi: 10.1039/C7TA05680J

Li, S., Dong, Y., Xu, L., Xu, X., He, L., and Mai, L. (2014). Effect of carbon matrix dimensions on the electrochemical properties of $Na_3V_2(PO_4)_3$ nanograins for high-performance symmetric sodium-ion batteries. *Adv. Mater.* 26, 3545–3553. doi: 10.1002/adma.201305522

Liang, J., Fan, K., Wei, Z., Gao, X., Song, W., and Ma, J. (2018a). Porous $NaTi_2(PO_4)_3$@C nanocubes as improved anode for sodium-ion batteries. *Mater. Res. Bull.* 99, 343–348. doi: 10.1016/j.materresbull.2017.11.030

Liang, J. J., Gao, X., Guo, J., Chen, C. M., Fan, K., and Ma, J. M. (2018b). Electrospun MoO_2@NC nanofibers with excellent Li^+/Na^+ storage for dual applications. *Sci. China. Mater.* 61, 30–38. doi: 10.1007/s40843-017-9119-2

Liang, J. J., Wei, Z. X., Wang, C. Y., and Ma, J. M. (2018c). Vacancy-induced sodium-ion storage in N-doped carbon nanofiber@MoS_2 nanosheet arrays. *Electrochim. Acta* 285, 301–308. doi: 10.1016/j.electacta.2018.07.230

Liang, J. J., Yuan, C. C., Li, H. H., Fan, K., Wei, Z. X., Ma, J. M. (2018d). Growth of SnO_2 nanoflowers on N-doped carbon nanofibers as anode for Li- and Na-ion batteries. *Nano Micro Lett.* 10:21. doi: 10.1007/s40820-017-0172-2

Longoni, G., Wang, J. E., Jung, Y. H., Kim, D. K., Mari, C. M., Ruffo, R. (2016). The $Na_2FeP_2O_7$-carbon nanotubes composite as high rate cathode material for sodium ion batteries. *Power Sourc J.* 302, 61–69. doi: 10.1016/j.jpowsour.2015.10.033

Lu, Y., Zhang, S., Li, Y., Xue, L., Xu, G., and Zhang, X. (2014). Preparation and characterization of carbon-coated $NaVPO_4F$ as cathode material for rechargeable sodium-ion batteries. *Power Sourc. J.* 247, 770–777. doi: 10.1016/j.jpowsour.2013.09.018

Pang, G., Nie, P., Yuan, C., Shen, L., Zhang, X., Li, H., et al. (2014a). Mesoporous $NaTi_2(PO_4)_3$/CMK-3 nanohybrid as anode for long-life Na-ion batteries. *J. Mater. Chem. A* 2, 20659–20666. doi: 10.1039/C4TA04732J

Pang, G., Yuan, C., Nie, P., Ding, B., Zhu, J., and Zhang, X. (2014b). Synthesis of NASICON-type structured $NaTi_2(PO_4)_3$-graphene nanocomposite as an anode for aqueous rechargeable Na-ion batteries. *Nanoscale* 6, 6328–6334. doi: 10.1039/C3NR06730K

Roh, H. K., Kim, M. S., Chung, K. Y., Ulaganathan, M., Aravindan, V., and Kim, K. B. (2017). A chemically bonded $NaTi_2(PO_4)_3$/rGO microsphere composite as a high-rate insertion anode for sodium-ion capacitors. *J. Mater. Chem. A* 5, 17506–17516. doi: 10.1039/C7TA05252A

Roy, P., and Srivastava, S. K. (2015). Nanostructured anode materials for lithium ion batteries. *J. Mater. Chem. A*, 3, 2454–2484. doi: 10.1039/C4TA04980B

Rui, X., Sun, W., Wu, C., Yu, Y., and Yan, Q. (2016). An advanced sodium-ion battery composed of carbon coated $Na_3V_2(PO_4)_3$ in a porous graphene network. *Adv. Mater.* 27, 6670–6676. doi: 10.1002/adma.201502864

Senguttuvan, P., Rousse, G., Arroyo, M., De Dompablo, Y., Vezin, H., Tarascon, J., et al. (2013). Low potential sodium insertion in NASICON-type structure through the Ti(III)/Ti(II). redox couple. *J. Am. Chem. Soc.* 135, 3897–3903. doi: 10.1021/ja311044t

Song, H., Li, N., Cui, H., and Wang, C. (2014). Enhanced storage capability and kinetic processes by pores- and hetero-atoms- riched carbon nanobubbles for lithium-ion and sodium-ion batteries anodes. *Nano Energ.* 4, 81–87. doi: 10.1016/j.nanoen.2013.12.017

Sun, D., Jin, G., Tang, Y., Zhang, R., Xue, X., Huang, X., et al. (2016). $NaTi_2(PO_4)_3$ nanoparticles embedded in carbon matrix as long-lived anode for aqueous lithium ion battery. *J. Electrochem. Soc.* 163, A1388–A1393. doi: 10.1149/2.1181607jes

Takashima, T., Tojo, T., Inada, R., and Sakurai, Y. (2015). Novel electrical energy storage system based on reversible solid oxide cells: system design and operating conditions. *Power Sourc. J.* 276, 113–119. doi: 10.1016/j.jpowsour.2014.11.109

Wan, M., Zeng, R., Chen, K. Y., Liu, G. X., Chen, W. L., and Huang, Y. H. (2018). Fe_7Se_8 nanoparticles encapsulated by nitrogen-doped carbon with high sodium storage performance and evolving redox reactions. *Energ. Storage Mater.* 10, 114–121. doi: 10.1016/j.ensm.2017.08.013

Wang, D., Liu, Q., Chen, C., Li, M., Meng, X., Bie, X., et al. (2016). NASICON-structured $NaTi_2(PO_4)_3$@C nanocomposite as the low operation-voltage anode material for high-performance sodium-ion batteries. *ACS Appl. Mater. Interf.* 8, 2238–2246. doi: 10.1021/acsami.5b11003

Wang, G., Zhang, S., Li, X., Liu, X., Wang, H., and Bai, J. (2018). Multi-layer graphene assembled fibers with porous structure as anode materials for highly reversible lithium and sodium storage. *Electrochim. Acta* 259, 702–710. doi: 10.1016/j.electacta.2017.11.039

Wang, H., Yu, W., Mao, N., Shi, J., and Liu, W. (2016). Effect of surface modification on high-surface-area carbon nanosheets anode in sodium ion battery. *Micropor. Mesopor. Mater.* 227, 1–8. doi: 10.1016/j.micromeso.2016.02.003

Wei, Z. X., Wang, L., Zhuo, M., Ni, W., Wang, H. X., and Ma, J. M. (2018). Layered tin sulfide and selenide anode materials for Li- and Na-ion batteries. *J. Mater. Chem. A* 6, 12185–12214. doi: 10.1039/C8TA02695E

Wu, C., Kopold, P., Ding, Y. L., Aken, P. A. V., Maier, J., and Yu, Y. (2015). Synthesizing porous $NaTi_2(PO_4)_3$ nanoparticles embedded in 3D graphene networks for high-rate and long cycle-life sodium electrodes. *ACS Nano* 9, 6610–6618. doi: 10.1021/acsnano.5b02787

Wu, X., Cao, Y., Ai, X., Qian, J., and Yang, H. (2013). A low-cost and environmentally benign aqueous rechargeable sodium-ion battery based on $NaTi_2(PO_4)_3$-$Na_2NiFe(CN)_6$ intercalation chemistry. *Electrochem. Commun.* 31, 145–148. doi: 10.1016/j.elecom.2013.03.013

Ye, S., Li, Z., Song, T., Cheng, D., Xu, Q., Liu, H., et al. (2017). Self-generated hollow NaTi2(PO4)3 nanocubes decorated with graphene as a large capacity and long lifetime anode for sodium-ion batteries. *RSC Adv.* 7, 56743–56751. doi: 10.1039/C7RA12291H

Zhang, F., Li, W., Xiang, X., and Sun, M. (2017). Nanocrystal-assembled porous $Na_3MgTi(PO_4)_3$ aggregates as highly stable anode for aqueous sodium-ion batteries. *Chem. Eur. J.* 23, 12944–12948. doi: 10.1002/chem.201703044

Zhao, B., Lin, B., Zhang, S., and Deng, C. (2015). A frogspawn-inspired hierarchical porous $NaTi_2(PO_4)_3$-C array for high-rate and long-life aqueous rechargeable sodium batteries. *Nanoscale* 7, 18552–18560. doi: 10.1039/C5NR06505D

Zhao, X., Yan, C., Gu, X., Li, L., Dai, P., Li, D., et al. (2017). Ultrafine TiO_2 nanoparticles confined in N-doped porous carbon networks as anodes of high-performance sodium-ion batteries. *Chem. Electro. Chem.* 4, 1516–1522. doi: 10.1002/celc.201700159

Zhou, D., Liu, Y., Song, W. L., Li, X., Fan, L. Z., and Deng, Y. H. (2017). Three-dimensional porous carbon-coated graphene composite as high-stable and long-life anode for sodium-ion batteries. *Chem. Eng. J.* 316, 645–654. doi: 10.1016/j.cej.2017.02.008

Conflict of Interest Statement: The authors declare that the research was conducted in the absence of any commercial or financial relationships that could be construed as a potential conflict of interest.